ADVANCED FUNCTIONAL MATERIALS
www.afm-journal.de

Organic Electrochemical Transistor Channel Materials: Copolymerization Versus Physical Mixing of Glycolated and Alkoxylated Polymers

Lize Bynens, Kaishuai Zhang, Priscila Cavassin, Arwin Goossens, Jochen Vanderspikken, Tania C. H. Castillo, Demetra Tsokkou, Adam Marks, Arianna Magni, Karrie Weaver, Laurence Lutsen, Sahika Inal, Koen Vandewal, Natalie Banerji, and Wouter Maes**

Organic electrochemical transistors (OECTs) feature a polymer channel capable of conducting both ions and electronic charges. The choice of the channel material is critical for OECT performance. Many efforts have focused on improving performance via the chemical tunability of conjugated polymers – through backbone, side chain, and molar mass engineering – leading to useful design principles for accumulation-mode OECT materials. However, tuning the chemical structure of conjugated polymers often requires time-consuming optimization of the synthesis route. Meanwhile, variations in molar mass, dispersity, structural defects, and metal content present challenges when attempting to analyze the detailed effects of structural modifications, as multiple performance-determining factors are often (unintentionally) changed at the same time. Therefore, this study explores blended channel materials obtained by physically mixing glycolated and alkoxylated polymers in different ratios, and compares their OECT performance with the corresponding statistical copolymers. It is shown that mixing two well-performing materials creates blends that enable rational tuning of the transistor properties without compromising on performance. Thus, channels based on blends of alkoxylated and glycolated polymers hold promise for OECT technology with tailored response, as only two materials are needed to achieve any desired side chain ratio, simplifying the optimization of OECT characteristics.

1. Introduction

Organic electrochemical transistors (OECTs) have emerged as a promising technology for a wide range of applications, such as biosensors, electrophysiology, and brain-computer interfaces.[1] Their potential in these fields stems from their unique operational principle, which relies on the ability of the channel material to conduct both electronic and ionic charge carriers. In OECTs, the electronic conductivity of this organic channel material is modulated by the ionic flux of an electrolyte resulting from a gate voltage modulation.[2] This provides several advantages over traditional organic solid-state transistors, such as low-voltage operation and high charge carrier mobility. Moreover, since OECTs are based on organic materials, they are fully printable and thus compatible with a wide range of substrates, including flexible, stretchable, and biocompatible materials, positioning them as ideal for use in wearable electronics, bio-sensing, and other applications that require conformable devices.[3]

L. Bynens, J. Vanderspikken, L. Lutsen, W. Maes
Institute for Materials Research (imo-imomec)
Design & Synthesis of Organic Semiconductors (DSOS)
Hasselt University
Martelarenlaan 42, Hasselt B-3500, Belgium
E-mail: wouter.maes@uhasselt.be

L. Bynens, A. Goossens, J. Vanderspikken, L. Lutsen, K. Vandewal, W. Maes
imec, imo-imomec
Wetenschapspark 1, Diepenbeek B-3590, Belgium

The ORCID identification number(s) for the author(s) of this article can be found under https://doi.org/10.1002/adfm.202423913

DOI: 10.1002/adfm.202423913

K. Zhang, P. Cavassin, D. Tsokkou, N. Banerji
Department of Chemistry
Biochemistry and Pharmaceutical Sciences
University of Bern
Freiestrasse 3, Bern 3012, Switzerland
E-mail: natalie.banerji@unibe.ch

A. Goossens, K. Vandewal
Institute for Materials Research (imo-imomec)
Organic Opto-Electronics (OOE)
Hasselt University
Martelarenlaan 42, Hasselt B-3500, Belgium

T. C. H. Castillo, S. Inal
Biological and Environmental Science and Engineering Division
Organic Bioelectronics Laboratory
King Abdullah University of Science and Technology (KAUST)
Thuwal 23955–6900, Saudi Arabia

A. Marks, A. Magni, K. Weaver
Department of Materials Science and Engineering
Stanford University
Stanford, California 94305, United States

OECT performance is quantified by the product of its electronic mobility and volumetric capacitance (μC^*). A high μC^* implies a more efficient OECT, as it indicates that the electronic charge carriers are easily transported through the channel material (μ) and that this material can store a substantial amount of ionic charges (C^*) to compensate for the electronic charges.[4] Another key performance metric is OECT stability under operating conditions.[5] Conjugated polymers present themselves as an ideal class of channel materials as they allow careful tailoring of the desired properties due to their large versatility in molecular design.[6] Because semiconducting polymers are typically hydrophobic, they are not very suitable for doping in aqueous electrolytes based on NaCl, often used to mimic biological systems. To achieve mixed conduction in accumulation-mode OECTs, hydrophilic analogs of established intrinsic semiconducting polymers are synthesized, most often by incorporating oligo(ethylene glycol) (OEG) side chains on the polymer backbone.[7]

However, replacing the hydrophobic side chains with glycol alternatives comes with some disadvantages. On the synthesis and characterization side, solubility issues are often encountered, complicating the synthetic protocols and purification steps, as well as hindering the molar mass determination of the final polymers.[8] Furthermore, it was shown by Moro et al. that glycol side chains do not interdigitate as well as alkyl chains, leading to a decreased tendency to form ordered assemblies, influencing the microstructure of these semiconducting polymers.[9] This can have a negative impact on the transport of electronic charge carriers. Therefore, it is interesting to design semiconducting polymers that contain both hydrophilic and hydrophobic side chains. Alkyl or alkoxy side chains can contribute to a higher degree of order in the polymer microstructure, which could lead to improved electronic transport.[9,10] Also, hydrophilic side chains significantly increase the amount of (passive) swelling in the film, which is detrimental for device stability.[11] Again, incorporating some hydrophobic side chains in the polymer channel material could mitigate this issue. Thus, there seems to be a trade-off between a high volumetric capacitance, achieved by hydrophilic side chains, and good electronic mobility and stability, promoted by hydrophobic side chains. Another important factor of OECT performance, also impacted by the type of side chain, is the response time.[12] Since OECT channel materials require doping by hydrated ions, a certain amount of glycolation is typically needed for effective doping. However, it has been shown that excessive glycolation can also negatively impact this figure of merit.[13]

Savva et al. previously reported an optimal glycol content in copolymerized materials to maximize both μC^* and the response time of OECTs.[13] They also showed that the threshold voltage (V_t) can be tuned by changing the ratio of OEG to alkoxy (OR) side chains. More recently, Siemons et al. reported an improvement of the electrochemical stability by incorporating 10% alkoxy side chains in a fully glycolated polymer.[11] It was shown via computational modeling that alkoxy side chains tend to afford aggregation in polar environments, resulting in alkyl-alkyl physical crosslinks in the channel material, hereby avoiding excessive swelling of the polymeric channel, which results in profound morphology changes upon in- and out-flux of ions and ultimately a decrease in device performance. These studies, along with other efforts to improve performance via side chain and molar mass engineering of conjugated polymers, has led to a set of useful design principles for p-type accumulation-mode OECT channel materials.[7c,14]

Apart from the synthetic challenges associated with side chain engineering,[15] the comparison of a series of copolymers with different side chains is complicated by variations in molar mass,[14h] dispersity, possible structural defects,[16] and residual metal content,[17] even when the polymerization approach is exactly replicated throughout the full series. These factors can play an important role in the eventual device performance, rendering direct comparison of OECT performances troublesome.[14h,17] In studies investigating the effect of different side chain ratios, the intermediate ratios are usually obtained using a three-monomer reaction. In a random copolymerization where both alkoxylated and glycolated monomers are incorporated, the resulting polymer chains will contain varying amounts of these units and are in essence a blend thereof. We therefore suspected blends of purely alkoxylated and glycolated polymers to perform similarly relative to their copolymer counterparts at comparable OEG:OR ratios. Furthermore, in a three-monomer reaction, it is difficult to know exactly how much of each monomer is built into the polymer and instead of the true side chain ratio, the monomer feed ratio is usually reported.[11,13] All these factors make it quite challenging to rationalize certain trends in a copolymer series. A solution for the laborious chemical modification of polymers and the previously mentioned drawbacks could lie in physically mixing two different polymers to attain a channel material with intermediate properties. It has been shown previously by Barker et al. that the use of conjugated polymer blends as a channel material enhances the response speed of OECT devices.[18] Also, Stein et al. have successfully employed polymer blends to achieve ambipolar OECTs and inverters.[19] However, the circumstances under which blended channel materials perform (at least) as well as their corresponding copolymer analogues have not yet been revealed.

To investigate if adjusting the ethylene glycol content of the channel material requires the synthesis of a new copolymer or can simply be achieved by mixing two polymers, in this work, a series of pBTTT[20] (poly(2,5-bis(3-alkylthiophen-2-yl)thieno[3,2-*b*]thiophene) like copolymers are synthesized, containing different ratios of ethylene glycol and alkoxy side chains. The fully glycolated pBTTT analog, pgBTTT, is currently one of the best-performing p-type accumulation-mode OECT materials.[21] However, the use of side chain variations to adapt the hydrophilicity of pgBTTT has not been investigated before. The copolymers are then compared to physical mixtures consisting of glycolated and alkoxylated polymers in the same OEG:OR side chain ratios to investigate whether polymer blending could be a suitable alternative to synthetically modifying the side chain ratio. One of the main advantages of blended channel materials is that any desired side chain ratio can be reliably obtained by mixing the same two polymers. The effect of mixing two materials instead of synthetically changing the polymeric channel material is thoroughly analyzed via grazing-incidence wide-angle X-ray scattering (GIWAXS), dynamic spectroelectrochemistry, electrochemical quartz crystal microbalance with dissipation monitoring (EQCM-D) measurements, and electrochemical and OECT stability testing. Our investigations reveal that physically mixing two high-performing OECT polymers results in blended channel

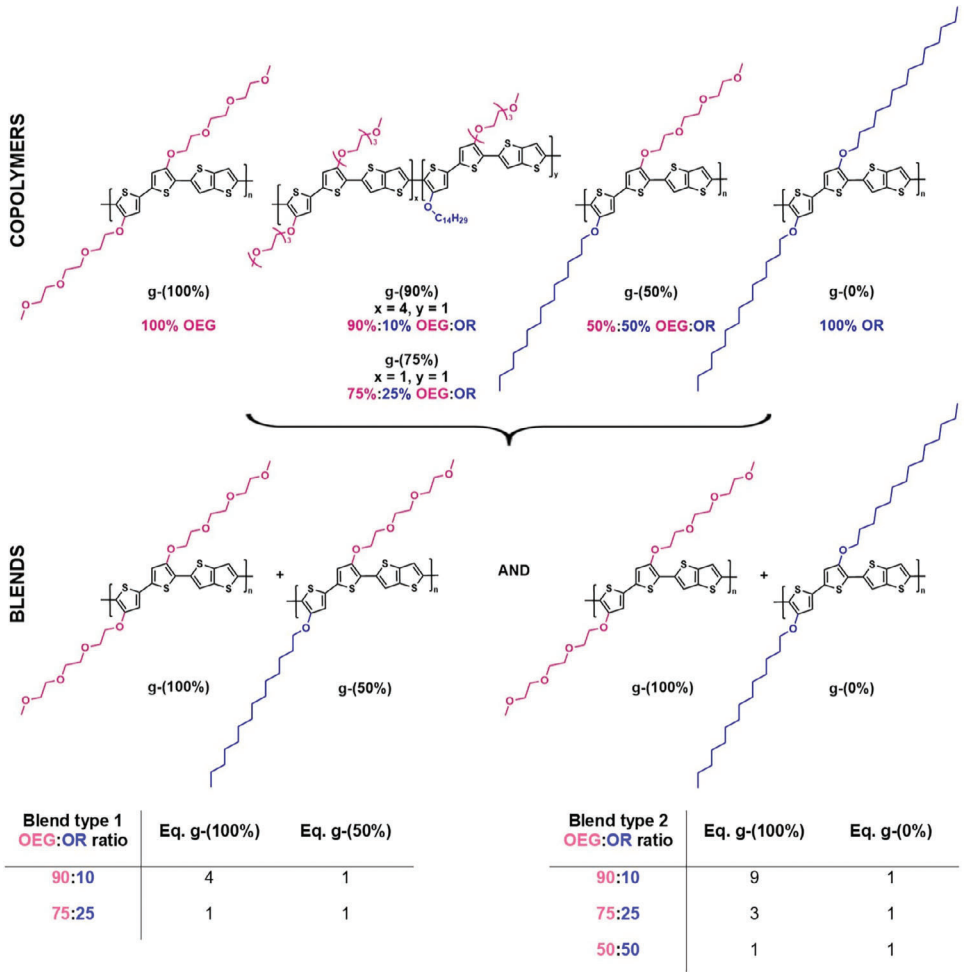

Blend type 1 OEG:OR ratio	Eq. g-(100%)	Eq. g-(50%)
90:10	4	1
75:25	1	1

Blend type 2 OEG:OR ratio	Eq. g-(100%)	Eq. g-(0%)
90:10	9	1
75:25	3	1
50:50	1	1

Figure 1. The investigated channel materials, consisting of the random copolymer series (top) and the physical blends (bottom). The g-(x%) nomenclature indicates the level of glycolation in the polymers. For the g-(90%) and g-(75%) copolymers, the feed ratios are reported, since these materials were synthesized via a three-monomer reaction. Further, a distinction is made between blends of g-(100%) with g-(50%) (type 1, left) and with g-(0%) (type 2, right). The desired OEG:OR ratios in the blends were obtained by mixing the respective polymers according to the equivalents (w/w%) indicated in the tables at the bottom.

materials that facilitate tuning of the transistor properties without compromising on performance or stability.

2. Results and Discussion

2.1. Polymer Synthesis and Characterization

Initially, a pBTTT-like copolymer series containing different ratios of randomly distributed OEG and OR side chains was prepared (**Figure 1**), similarly to the study of Savva et al., where they synthesized the following OEG:OR ratios: 100:0, 75:25, 50:50, and 0:100.[13] However, in our series, a 90:10 OEG:OR ratio was incorporated as well, since it was proven to be a beneficial side-chain ratio by Siemons et al.[11] Also, pgBTTT (poly(2-(4,4′-bis(2-(2-(2-methoxyethoxy)ethoxy)ethoxy)-[2,2′-bithiophen]-5-yl)-*alt*-thieno[3,2-*b*]thiophene)) was used as the fully glycolated reference polymer instead of its regioisomer pg2T-TT (poly(2-(3,3′-bis(2-(2-(2-methoxyethoxy)ethoxy)ethoxy)-[2,2′-bithiophen]-5-yl)-*alt*-thieno[3,2-*b*]thiophene)) because of its superior performance, attributed to a higher hole mobility due to improved planarity of the polymer backbone.[21] By adding alkoxy side chains we can investigate if the charge transport improves due to a potential increase in microstructural order. The polymer backbone with alternating thienothiophene and bithiophene units remains untouched throughout the full series to only probe for the influence of the hydrophobic/hydrophilic character in a top-performing p-type OECT material.

The copolymer series was then compared to physical mixtures consisting of the fully glycolated polymer (g-(100%)) and the 50% glycolated polymer (g-(50%)) and to mixtures consisting of g-(100%) and the fully alkoxylated polymer (g-(0%))[22] in the same OEG:OR side chain ratios (Figure 1). Thus, a distinction is made between two different types of blends. Blends of type 1 (g-(100%) + g-(50%)) are expected to be nicely intermixed and well-performing, since both polymers are hydrophilic and produce good OECTs when used as the single channel material (Figure S14, Supporting Information). The comparison is made with blends of type 2 (g-(100%) + g-(0%)). The latter fully

alkoxylated polymer is hydrophobic, which could influence the miscibility with g-(100%). Also, no operational OECTs could be made with g-(0%) as the single channel material in contact with a 0.1 M NaCl electrolyte (Figure S14, Supporting Information). It was previously reported by Giovannitti et al. that the low degree of swelling and ionic conduction in hydrophobic polymers increases the required oxidation voltage, in turn leading to device degradation or non-operational OECTs.[7a,13]

NMR spectroscopy analysis was performed on the highest molar mass (chloroform) fractions of the polymers after Soxhlet extractions. From the NMR spectra (Figures S3–S7, Supporting Information), it is clear that the OEG:OR ratio decreases throughout the series, from g-(100%) to g-(0%). The NMR signal representing most of the alkoxy side chain protons (1.5-1.25 ppm), excluding the methylene protons adjacent to the oxygen atom, grows when the share of hydrophobic side chains increases. Integration of this signal compared to the signal representing the glycol side chain protons roughly confirms the OEG:OR ratios in the different copolymers. However, it has to be taken into account that quantitative analysis of NMR spectra of conjugated polymers is difficult due to solubility issues, signal broadening, and a pronounced H_2O signal, rendering the exact integration not as reliable as for small molecules.[16]

A common challenge in the field, that was also faced during this study, is the molar mass determination of glycolated conjugated polymers.[6,8,23] Various gel permeation chromatography (GPC) systems were tried, but none provided reliable results (SI, section 2). Therefore, we resorted to estimating molar mass using MALDI-ToF (matrix-assisted laser desorption/ionization – time-of-flight) mass spectrometry (MS) (Figures S8–S12, Supporting Information), despite its clear limitations,[24] to gauge the comparability of the chain lengths of the various polymers.[25] From the mass spectra, all polymers seem to have a comparable mass distribution, except for g-(75%), where the chloroform fraction gave little to no signal. This could be an indication that g-(75%) is a higher molar mass polymer, since it has been reported that at higher polydispersities (PD > 1.2), the high-mass components are generally underrepresented in MALDI-ToF MS.[24,26] To address this, a lower molar mass sample of g-(75%) was measured instead. It was obtained via Soxhlet extractions, which were used to purify all polymers, resulting in distinct molar mass fractions. Before chloroform, which eluted the highest molar mass fractions for all polymers, tetrahydrofuran (THF) was used, in which the second highest molar mass fraction was obtained. For g-(75%), this fraction was analyzed with MALDI-ToF MS instead. For all further experiments, the chloroform fractions of all polymers were used, so it has to be taken into account that g-(75%) is likely of higher molar mass than the other polymers in the series when comparing the results. This issue illustrates that obtaining a similar molar mass for all copolymers in a series is rather challenging, even when using the exact same reaction conditions.

UV-Vis absorption spectroscopy analysis of the polymers and the blends was then performed on completely dedoped films in electrolyte solution (Figure S13a, Supporting Information), with all the absorption maxima situated between 600 and 605 nm. Hence, λ_{max} is not significantly affected by the ratio of ethylene glycol to alkoxy side chains. However, small changes are seen in the ratio of the 0-0 (with a maximum at 650 nm) and the 0–1 (with a maximum at 600 nm) vibronic bands when comparing the materials. A higher 0-0 to 0–1 ratio indicates the presence of more planar polymer chains, which suggests a significant intrachain order that favors electronic delocalization along the polymer chain.[27] The enhanced chain ordering in certain compositions is also consistent with tight π-π stacking, ultimately leading to a crystalline phase that might either boost device performance by improving the carrier mobility or rather limit performance because it restricts ion accessibility between the side chains, affecting the doping efficiency of the material.[27b] Among the copolymers, only the g-(75%) copolymer exhibits a more pronounced 0-0 vibronic band compared to g-(100%), which might relate to a better polymer packing in the film, consistent with the assumed higher molar mass of g-(75%) (Figure S13b, Supporting Information). We observe that the type 2 blends (g-(100%) + g-(0%)) show similar absorption spectra to the copolymers, with a weaker 0-0 vibronic band, which suggests their morphology is similar (Figure S13b,c, Supporting Information).[28] In addition, the type 1 blends (g-(100%) + g-(50%)) have a slightly higher ratio between the 0-0 to 0–1 vibronic bands compared to blends with g-(0%), indicating a higher degree of order which would predict increased mobilities (Figure S13d, Supporting Information).

2.2. OECT Performance

To compare the device performance of the copolymers and blends as channel materials in OECT devices, their transistor characteristics were determined. The transconductance, g_m, was extracted and describes the extent to which an OECT can amplify a gate voltage signal ($g_m = \frac{\partial I_d}{\partial V_g}$). In the saturation regime, g_m depends on specific device characteristics according to Equation (1):[29]

$$g_m = \frac{Wd}{L}\,\mu C^*\left(V_t - V_g\right) \tag{1}$$

In this equation, W, d, and L are the width, thickness, and length of the channel, respectively, V_t is the threshold voltage, and V_g is the applied gate voltage. In the OECT field, the mobility-capacitance product (μC^*) is generally used to compare different channel materials.[4,30] In this work, μC^* was extracted from the slope of the linear extrapolation of the square root of the saturated transfer curves at a V_d of -0.6 V according to Equation (2):

$$\sqrt{I_d^{sat}} = \sqrt{\frac{Wd}{2L}\mu C^*}\cdot\left(V_t - V_g\right) \rightarrow slope = \sqrt{\frac{Wd}{2L}\mu C^*} \leftrightarrow \mu C^* = \frac{2L}{Wd}\cdot slope^2 \tag{2}$$

Very high μC^* values were obtained, ranging from 960 ± 160 F cm^{-1} V^{-1} s^{-1} to 2420 ± 250 F cm^{-1} V^{-1} s^{-1} for the full series. However, it is important to recognize that direct comparison with literature values may not be entirely appropriate, as discussed by Shahi et al., since the μC^* product reflects a device-specific characteristic rather than an intrinsic material property.[31] Nonetheless, given that consistent measurement conditions and device parameters were maintained in our study, the μC^* product remains a reliable indicator to establish trends within our material series.

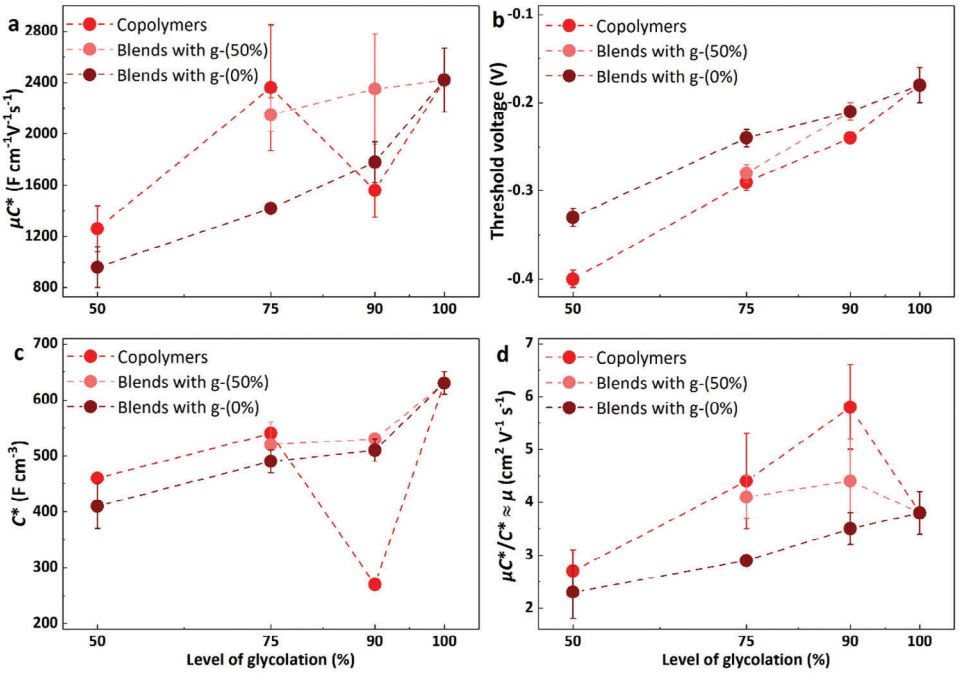

Figure 2. Overview of the OECT characteristics for the copolymers, type 1 blends (g-(100%) + g-(50%)) and type 2 blends (g-(100%) + g-(0%)): a) μC^* extracted from the slope of the linear extrapolation of the square root of the saturated transfer curves at a V_d of −0.6 V, b) V_t extracted from fits of $I_d^{1/2}$ vs. V_g plots, c) C^* independently determined by chronoamperometry (Figures S16–S18; Tables S5–S7, Supporting Information), and d) Inferred μ determined by dividing μC^* by C^*. Reported uncertainties are one standard deviation with n = 2–3 devices with different channel dimensions, T1 (LxW = 2 × 3 mm) and T2 (LxW = 0.5 × 5.5 mm).

An overview of all the parameters extracted from the OECT measurements is shown in **Figure 2** and in the Supporting Information (Tables S2–S4; Figure S14, Supporting Information). The figure of merit μC^* for g-(100%) is 2420 ± 250 F cm^{-1} V^{-1} s^{-1}. Using chronoamperometry, a C^* value of 630 ± 20 F cm^{-3} is obtained, from which an OECT mobility of 3.8 ± 0.4 cm^2 V^{-1} s^{-1} can be estimated. In the original study on pgBTTT, a C^* and μ value of 164 ± 7 F cm^{-3} and 3.44 ± 0.13 cm^2 V^{-1} s^{-1} were reported, respectively.[21] The higher μC^* for our pgBTTT batch can thus mainly be attributed to an increase in C^*. However, it is important to note that the experiments on original pgBTTT were performed on µm-scale devices, while in our study, mm-scale devices were used. Also, in this study, higher gate potentials were generally applied, so the measuring conditions were not exactly replicated.

In the copolymer series, a peculiar trend in μC^* was established (Figure 2a). Namely, μC^* for g-(90%) drops quite drastically to 1560 ± 210 F cm^{-1} V^{-1} s^{-1}, which is unexpected, given that only 10% of ethylene glycol side chains are switched to alkoxy chains. On the other hand, the g-(75%) polymer has a μC^* similar to that of g-(100%), namely 2360 ± 490 F cm^{-1} V^{-1} s^{-1}. This can probably be attributed to its higher molar mass. The OECT performance dependency of g-(75%) on molar mass was analyzed by measuring the transistor characteristics of the lower molar mass (THF) fraction of this polymer, which was also used for MALDI-ToF analysis (Figure S10, Supporting Information), resulting in a quite drastic drop in performance (μC^* = 940 ± 110 F cm^{-1} V^{-1} s^{-1}). Polymer g-(50%) has the lowest μC^* in the series, namely 1260 ± 180 F cm^{-1} V^{-1} s^{-1}. Based on previous literature,[13] a decrease in C^* is expected with an increasing amount of alkoxy side chains due to the hydrophobic nature of these chains, which impedes water uptake.[7a] However, in this copolymer series, this predicted trend does not hold true (Figure 2c), which also makes the trend in inferred mobility more difficult to explain (Figure 2d). The lack of a clear, predictable trend of the transistor characteristics in the copolymers could have different origins. First, if the polymers are not of similar molar mass, OECT performances cannot be directly compared.[14h] Second, batch-to-batch variations in dispersity, possible structural defects, and residual metal content can affect the device performance further, even if the synthetic method is exactly replicated within a series.[16,17] These factors make it difficult to compare a series of copolymers and justify our approach to use blends instead.

When using the blends as channel materials in the OECTs, the trends are clearer. As expected, C^* decreases slightly with an increasing amount of alkoxy side chains, but remains relatively high, with values above 400 F cm^{-3} (Figure 2c). Concerning the inferred hole mobility, for the blends with g-(50%), μ slightly increases when alkoxy side chains are introduced in the channel material, with the optimum situated at 10%. However, blends with g-(0%) show a gradual decrease in μ with increasing fraction of hydrophobic side chains, indicating that the expected improvement in polymer packing does not occur (Figure 2d). Overall, blends with g-(50%) have high μC^* values, comparable to g-(100%) as the sole channel material, while blends with g-(0%) show a gradual decline in μC^* when more g-(0%) is incorporated (Figure 2a).

When comparing the threshold voltages of all the materials, it is observed that a larger voltage needs to be applied for an increasing amount of hydrophobic side chains in all cases (Figure 2b). This follows the expected trend, since the alkoxy side chains do not allow ion penetration as easily, requiring larger gate voltages to dope the polymer channels.[7a,13] For channel materials that have the same level of glycolation, V_t is of the same order of magnitude. However, it can be noted that the increase in V_t is slightly more gradual in the blends compared to the copolymers.

By conducting time-resolved OECT measurements, the time constants (τ) of the various channel materials were determined from the transient drain current curves after applying a square voltage pulse at an overpotential of −0.2 V (Figure S15, Supporting Information). Notably, the introduction of alkoxy side chains in the copolymers resulted in a decreased turn-on time for the OECT, with an optimal reduction observed at 10% alkoxy chains. For the blended channel materials, a similar trend was observed. Compared to neat g-(100%), τ generally decreases when alkoxylated polymers are incorporated in the blends, although these changes were again more gradual than for the copolymers.

Thus, it is clear that blending two polymers is a valid strategy to adapt certain transistor characteristics (e.g. V_t, μ, τ), while maintaining highly performant devices. The blends with g-(50%) generally perform better and have faster response times than the blends with g-(0%), especially when the amount of alkoxy side chains increases. This was to be expected, since g-(50%) is a good channel material on its own, while no working OECTs could be made with g-(0%) as the sole channel polymer in contact with a 0.1 M NaCl electrolyte because of its hydrophobic nature.[7a] When comparing the copolymers to the blends with the same side chain ratios, it is clear that the μC^* values lie within the same range. However, blending two polymers is a more accessible strategy than copolymerization, since the same two materials can be used to reliably obtain any desired ratio of side chains. This way, the synthetic effort toward an extensive series is significantly reduced, as well as the batch-to-batch variations within that series, making it easier to predict and design certain trends.

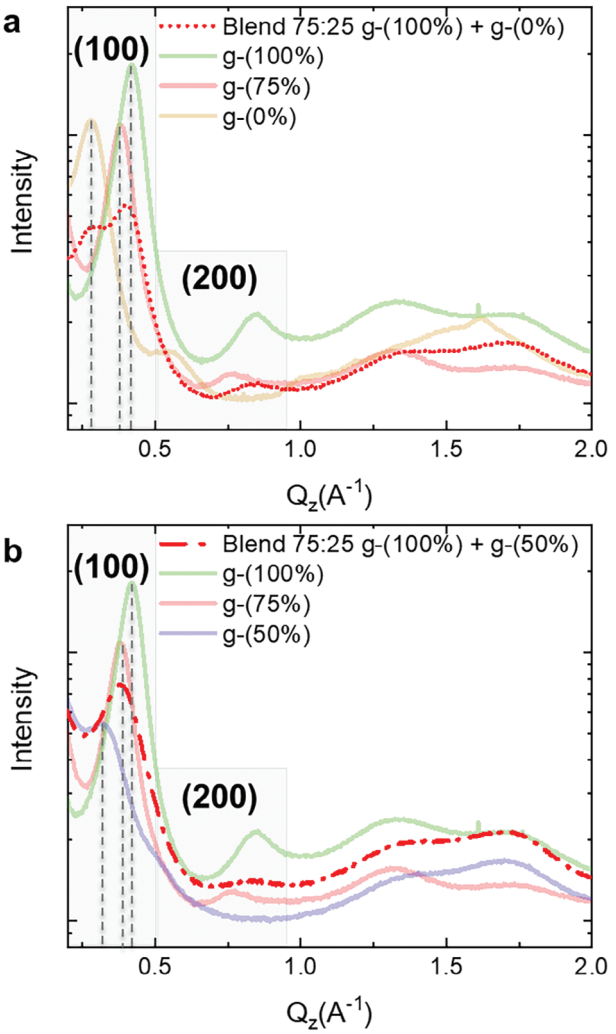

Figure 3. a) Q_z lineout for the type 2 75:25 blend (g-(100%) + g-(0%)), showing two (100) lamellar peaks whose maxima align with those of the neat polymers. b) Q_z lineout for the type 1 75:25 blend (g-(100%) + g-(50%)), where the lamellar peak coincides with g-(75%). Dashed lines are a guide for the eye only. Grey areas highlight the regions in which the (100) and (200) lamellar peaks appear.

2.3. Film Microstructure

To understand the effect of the varying OEG:OR content in the copolymers and the respective blends on the film microstructure, GIWAXS analysis was performed. The g-(0%), g-(50%), g-(75%), and g-(100%) polymers and the 75:25 blends of type 1 and 2 were analyzed and compared. The 2D plots, lineouts, and a peak annotation table can be found in the SI (Figures S19 and S20; Table S8, Supporting Information). Whereas g-(100%) and g-(75%) present themselves as more edge-on, g-(50%), g-(0%), and both blends show a mixed edge- and face-on orientation toward the substrate. As is typical for these materials,[16a,21] clear (100) and (200) lamellar peaks can be observed in Q_z (**Figure 3**) but not in Q_{xy}, indicating the absence of lamellar order in the in-plane direction, consistent with literature.[21] All copolymers containing alkoxy side chains show an attenuation in the (200) peak compared to g-(100%). However, the (200) peak is more pronounced for g-(75%) than for g-(50%) and g-(0%), indicating slightly better long-range order, possibly originating from a higher molar mass. Due to the shorter ethylene glycol side chains and their different interdigitation behavior, the g-(100%) (100) lamellar stacking peak appears at 0.42 $Å^{-1}$ (15.0 Å), whereas for g-(0%), with alkoxy side chains, it appears at 0.28 $Å^{-1}$ (22.4 Å), consistent with literature.[16a,21] Copolymers g-(75%) and g-(50%) demonstrate intermediate values of 0.38 $Å^{-1}$ (16.5 Å) and 0.32 $Å^{-1}$ (19.6 Å), respectively (Figure S21, Supporting Information). Despite the incorporation of both alkoxy and glycol side chains in the copolymers, the (100) lamellar stacking peaks appear featureless (one single peak; Figure 3), similarly to what was observed by Savva et al. for the p(2T-TT) regioisomer.[13] This suggests that there are no large individual crystallites with dominant alkoxy or glycol-decorated chains. Likewise, the type 1 75:25 blend (g-(100%) + g-(50%)) shows a single peak at 0.38 $Å^{-1}$ (16.5 Å), the same value as obtained for g-(75%) (Figure 3b). However, the type 2 75:25 blend (g-(100%) + g-(0%)) does show two distinguishable (100) lamellar stacking peaks with maxima at 0.28 $Å^{-1}$ (22.4 Å) and 0.40 $Å^{-1}$ (15.7 Å), in accordance

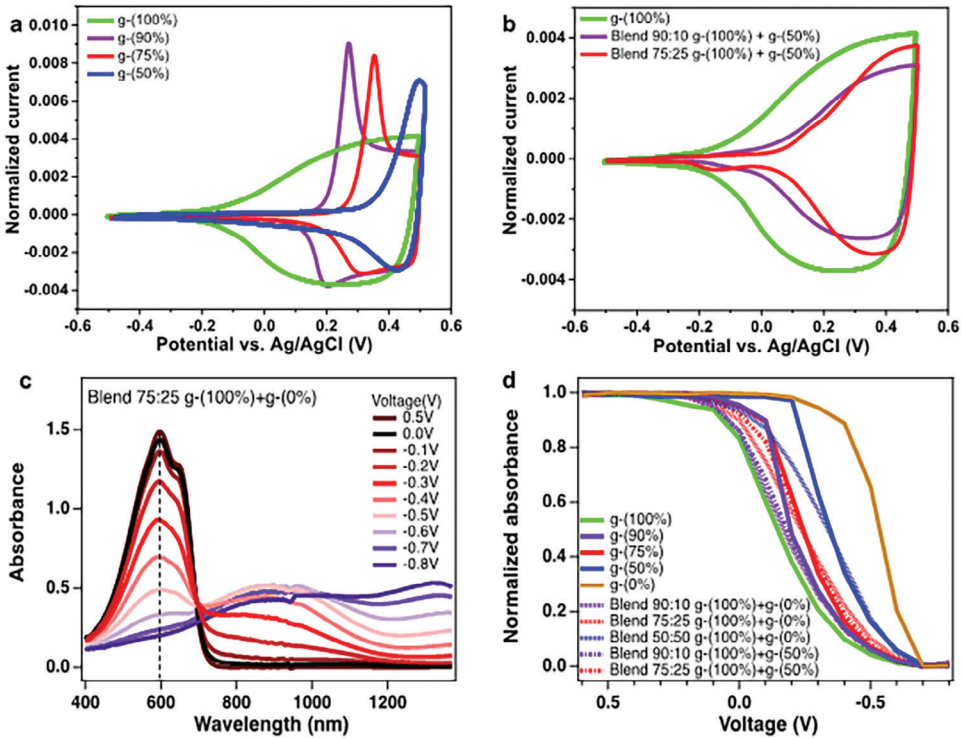

Figure 4. Electrochemical characterization and optical response of the copolymer and blend systems: a) Cyclic voltammograms for the copolymers conducted at 100 mV s^{-1} in 0.1 M aqueous NaCl electrolyte, normalized by layer thickness for cross-sample analysis. b) Cyclic voltammograms for the type 1 blends (g-(100%) + g-(50%)) in the same side chain ratios as (a). c) Steady-state Vis-NIR electrochemical absorbance spectra at different applied voltages for type 2 blend 75:25 (g-(100%) + g-(0%)) (film thickness = 112 nm) from +0.5 to −0.8 V, showing doping-induced spectral changes; a dwell time of 30 s was used at each voltage. d) Neutral absorbance band evolution at 600 nm (scaled between 0 and 1) for the copolymers and blends as a function of applied voltage from +0.5 to −0.8 V.

with the values obtained for the neat polymers (Figure 3a). This indicates that, on a microstructural level, the film contains alkoxylated and glycolated polymer crystallites and is less intermixed as compared to the type 1 blend. As the backbone is the same for all materials, the (010) π-π peak appears at very similar values (1.74-1.67 $Å^{-1}$; 3.6-3.7 Å) for both the (co)polymers and the blends (Figure S20; Table S8, Supporting Information).

The differences in intermixing between the type 1 and type 2 blends account for the variations in OECT performance and UV-Vis absorption spectra. Type 1 blends, consisting of two hydrophilic polymers (g-(100%) and g-(50%)), exhibit better intermixing, resulting in a more organized structure. This is evidenced by the higher 0-0 to 0–1 vibronic band ratio (Figure S13, Supporting Information) and increased μ values, which lead to a higher μC^* (Figure 2a,d). In contrast, type 2 blends, comprising a hydrophilic (g-(100%)) and a hydrophobic polymer (g-(0%)), show less favorable intermixing, explaining the steeper decrease in μC^* when more g-(0%) is incorporated in the blends (Figure 2a).

2.4. Electrochemical and Swelling Behavior

The electrochemical properties of the copolymers and blends were probed with aqueous cyclic voltammetry, spectroelectrochemistry, and EQCM-D. The oxidation onsets ($E_{ox,onset}$) were extracted from the voltammograms (**Figure** 4a,b; Figure S22, Supporting Information) and are shown in **Table** 1.

The expected trend, an increasing oxidation onset with increasing amount of alkoxy side chains, is observed for both the pure

Table 1. Oxidation onsets ($E_{ox,onset}$) extracted from the cyclic voltammograms for the pristine copolymers and the blends, and quantification of the electrochemical doping extent based on 50% of absorbance loss at 600 nm (neutral species, $V_{abs,50\%}$).

$E_{ox,onset}$	g-(100%)	90:10	75:25	50:50	
Copolymers	−0.11 V	0.20 V	0.28 V	0.36 V	
Type 1 blends g-(100%) + g-(50%)	/	0.04 V	0.09 V	/	
Type 2 blends g-(100%) + g-(0%)	/	−0.02 V	0.07 V	0.08 V	
$V_{abs,50\%}$	g-(100%)	90:10	75:25	50:50	g-(0%)
Copolymers	−0.15 V	−0.20 V	−0.24 V	−0.35 V	−0.53 V
Type 1 blends g-(100%) + g-(50%)	/	−0.18 V	−0.24 V	/	/
Type 2 blends g-(100%) + g-(0%)	/	−0.17 V	−0.23 V	−0.34 V	/

materials and the blends. It was previously reported by Savva et al.[13] that the ratio of OEG:OR side chains impacts the amount of swelling and ion penetration, thereby changing the oxidation onsets and hence the threshold voltages. Indeed, the EQCM-D data show reduced swelling when alkoxy side chains are introduced (vide infra). In the copolymers, the shift to higher $E_{ox,onset}$ values upon adding more alkoxy side chains is most pronounced, while the blends show a more gradual increase. This is to be expected based on the similar behavior of the OECT threshold voltages (Figure 2b). When looking at the shape of the voltammograms in Figure 4a,b and S22 (Supporting Information), a clear difference can be seen between the copolymers and the blends. As soon as alkoxy side chains are introduced in the copolymers, the shape of the oxidation curve drastically changes. Instead of a gradual current increase, as for g-(100%), the curve remains flat until the oxidation onset is reached, after which it achieves its maximal current almost instantaneously, causing a sharp oxidation onset. This is a desired feature for transistor materials, since the devices often need to operate as efficient switches.[32] On the contrary, the voltammogram shapes for the blend series all resemble the shape of the g-(100%) curve, even when alkoxylated polymers are included in the mixtures. This behavior might be associated with a larger spread of local energetics, i.e. of polymer segments having slightly different oxidation onsets, in the fully glycolated polymer and the blends.

To gain further insights into the doping mechanisms of the channel materials, we delved into the optical properties upon electrochemical doping of the copolymers and blends, by measuring the evolution of the steady-state absorbance at different voltages to vary the doping level.[33] For this, the channel materials were deposited on indium tin oxide (ITO) substrates. We used 0.1 M aqueous NaCl electrolyte and the voltages were progressively applied from +0.5 to −0.8 V in −0.1 V steps with a dwell time of 30 seconds (Figures S25 and S26, Supporting Information). Note the inversion of the sign compared to cyclic voltammetry, which is simply a difference in convention in describing the oxidation potential during electrochemical and OECT (and spectroelectrochemical) measurements. To show the reproducibility and reliability of our findings, similar measurements were performed on OECTs under comparable experimental conditions, which revealed an almost identical behavior at all voltages, such as consistent doping levels and similar absorbance bands (Figures S23 and S24, Supporting Information).[33,34] Since all materials are slightly doped in ambient conditions, a positive gate voltage between +0.5 to +0.6 V was applied after every measurement to fully dedope the copolymers and blends and prove the reversibility of the doping/dedoping process.

As an example, the absorbance spectra for the type 2 75:25 blend (g-(100%) + g-(0%)) at different voltages are shown in Figure 4c, while the results for the other materials are included in Figure S26 (Supporting Information). At +0.5 V, only the absorbance from the neutral species is present, which exhibits a Gaussian-like shape with a peak around 600 nm and an adjacent shoulder at ≈650 nm, characteristic of the 0-0 and 0–1 absorption bands of the polymer, as discussed above.[27] The feature predominantly comprises $\pi \rightarrow \pi^*$ transitions coupled with the C=C stretching modes of the thiophene rings. This absorption band undergoes noticeable attenuation as the voltage becomes more negative. Simultaneously, we observe the emergence of new broad absorption bands with a maximum at ≈950 and 1350 nm, indicative of the polymer's oxidation and the formation of oxidized species, polarons and bipolarons, respectively.[35] As the voltage decreases, first the polaronic band at 950 nm increases, while at more negative voltages it reaches its maximum and then decreases again, with the concomitant rise of the absorbance band at 1350 nm due to the formation of bipolaronic species. At the most negative voltages, we observe the polaron decrease and bipolaron rise for all copolymers and blends, showing that a similar doping extent and high doping level is reached (Figure S26, Supporting Information). Exceptions to this are g-(0%) and the type 2 blend 50:50 (g-(100%) + g-(0%)), where this high doping level can't be obtained, as the polaron band saturates at the most negative voltages but does not decrease. This can be justified by the higher oxidation onset of the g-(0%) copolymer.

In Figure 4d, we plot the evolution of the neutral absorbance band (at 600 nm) as a function of voltage for the copolymers and blends. For each system, the absorbance value at the most negative voltage was subtracted, thereby anchoring its lowest value to zero, followed by normalization at the maximum value. This step re-scales all traces between 0 to 1 to enable a comparative analysis between the different channel materials. Through this analysis, we assess the polymers' optical onset voltage ($E_{op,onset}$) and the voltage inducing a 50% change in neutral absorbance ($V_{abs,50\%}$) (Table S9, Supporting Information and Table 1, respectively). The optical onset is quite scattered due to the relatively large voltage steps (0.1 V) and the wider spread oxidation range for the blends compared to the copolymers. However, the $V_{abs,50\%}$ reveals a clear trend, as such that the increase of alkoxy side chains leads to an increase in the negative voltage required to deplete the neutral peak, similar to the results obtained from cyclic voltammetry.[24] Interestingly, we see similar $V_{abs,50\%}$ values for the copolymers and two corresponding blends with the same ratio of OEG:OR side chains, showing their comparable electrochemical behavior and overall energetics.

EQCM-D measurements were carried out on selected samples in 0.1 M aqueous NaCl electrolyte, namely g-(100%), g-(75%), and type 1 blend 75:25 (g-(100%) + g-(50%)) (Figures S31–S34, Supporting Information). As seen in **Figure 5**, both the passive (without applied voltage) and the active swelling (during electrochemical doping) are reduced in both samples containing 25% alkoxy side chains. This confirms our hypothesis that the addition of hydrophobic side chains reduces swelling, no matter whether copolymerization or blending is used. Still, both channel materials demonstrate important mass uptake when the oxidation voltage increases (Figure 5b), in line with efficient electrochemical doping. Moreover, the similar properties of the copolymer and the type 1 blend with 25% alkoxy side chains are highlighted by their very comparable swelling level, confirming once more that blending two well-performing OECT materials is an effective alternative to copolymerization.

2.5. Doping Dynamics

Building on the steady-state and voltage-dependent insights, our investigation was then extended to the time-resolved electrochemical and optical behavior of the copolymers and blends (**Figure 6**). Figure 6a shows the absorbance spectra of the type

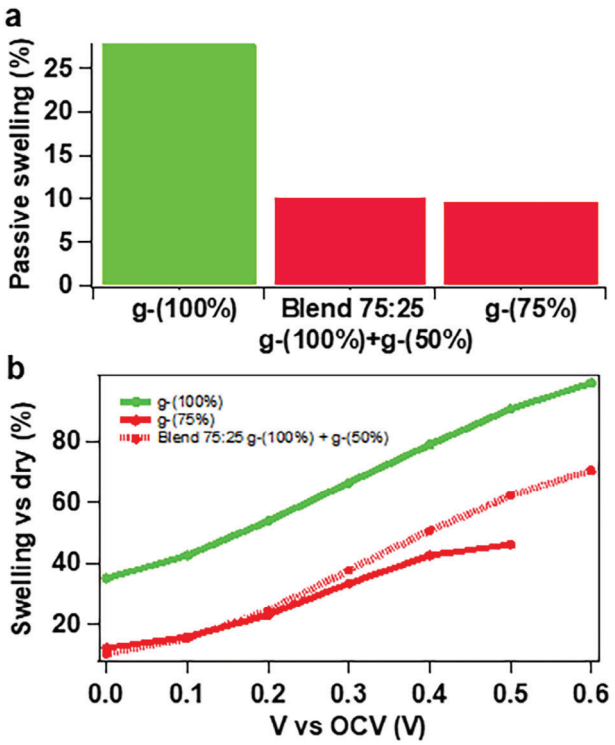

Figure 5. EQCM-D measurements in 0.1 M aqueous NaCl electrolyte, obtained for g-(100%), g-(75%), and type 1 blend 75:25 (g-(100%) + g-(50%)). a) Shows the passive swelling without applied voltage, while b) shows the active swelling during electrochemical doping.

2 75:25 blend (g-(100%) + g-(0%)) at different times, from 0 to 10 s after a voltage switch from +0.5 to −0.9 V. The dynamics highlight the gradual transition from neutral species through polarons to bipolarons within the observed timeframe. At time zero, the spectrum shows only neutral polymer,[27] and then the doping process evolves and the neutral band is depleted. In parallel, broad absorption bands emerge at longer wavelengths. The different temporal progression between the band peaking at 950 nm (polarons) and the one at 1350 nm (bipolarons) reveals that the formation of polarons takes place within 1.5 s, followed by evolution to bipolarons until 10 s.[36]

The doping dynamics in the copolymers and blends were compared by monitoring the temporal evolution of the neutral absorbance band at 600 nm. In general, the doping kinetics are influenced by factors such as the ion and hole mobility, the film morphology, the rate of the electrochemical oxidation, and the concomitant polymer backbone rearrangements.[37] For comparative analysis between the different materials, films of similar thickness (≈50 nm) were used and the final voltage was always chosen to be −0.4 V below $V_{abs,50\%}$ (Table 1). This allows taking into account the shift in oxidation potential and enables comparison between similar doping levels. In Figure 6b, we compare the neutral decay dynamics of all the copolymers. The polymers with high OEG content, g-(100%), g-(90%), and g-(75%), all exhibit fast and relatively similar doping dynamics (time constant of 0.30–0.53 s, **Table 2**). Close inspection reveals that the doping is slightly faster in g-(90%), which agrees with the OECT drain current transients discussed above. It is likely related to improved hole mobility (with reduced swelling due to the alkoxy side chains), combined with favorable ionic transport.

However, as the amount of glycol side chains is further reduced in g-(50%) and g-(0%), the dynamics significantly slow down (Figure 6b). Notably, the fully alkoxylated copolymer, g-(0%), dopes with a time constant of ≈5 s, which is 15 times slower than the doping speed for the fully glycolated polymer, g-(100%) (Table 2). The dynamics of the polarons at 950 nm and of the bipolarons at 1350 nm show exactly the same trend between the different copolymers, with doping being fastest in g-(90%) and slowest in g-(0%) (Figure S27, Supporting Information). The spectro-electrochemical measurements optically detect the doping, and in this set-up, the doping rate is particularly sensitive to ion transport through the thickness of the film, as the holes are injected from the ITO directly underneath the film. In contrast, the transient drain current measures not only the doping rate, but also the current flow across the large channel and any resistance at the contacts, which might explain the slightly different trends with glycolation (Figure S15, Supporting Information).

As the blends contain components with strongly different doping dynamics, any significant phase separation of the constituent polymers could lead to strongly biphasic behavior with fast (for the OEG-rich phase) and slow (for the alkoxy-rich phase) dynamics. In Figure 6c, we compare the neutral, polaron and bipolaron dynamics of the g-(75%) copolymer with the two corresponding 75:25 blends, involving g-(100%) mixed with either g-(50%) or g-(0%). We observe comparable dynamics for the three samples, which are almost as fast as in g-(100%) and do not show significantly slow components related to the alkoxy side chains. In Figure S28 (Supporting Information), the g-(50%) and g-(90%) copolymers are compared to their corresponding blends, and again, the dynamics are relatively similar. For each glycol ratio, the differences between the two blends and the copolymer are much smaller than the differences between the individual blend components. The precise dynamics in each sample are likely affected by subtle changes in their morphology, which will be investigated in more detail in a follow-up study. The trends with increasing alkoxy content in the blends reflect the ones of the copolymers: samples with a 90:10 OEG:OR ratio are always fastest and the doping slows down significantly in the least glycolated samples (Table 2). Overall, our observations confirm sufficient intermixing of the glycolated and alkoxylated polymers in both blend types, so that they adopt an overall comparable behavior as the copolymers.[38] This reinforces the notion that the mixed ionic-electronic conduction between copolymers and blends is comparable.

2.6. Stability

To investigate the stability of the polymer channels and determine if the stability of the blends matches that of the copolymers, we examined the stability of g-(100%) and compared it to g-(90%) and the type 1 blend 90:10 (g-(100%) + g-(50%)). First, we focused on the electrochemical stability. The 90:10 ratio of glycol to alkoxy side chains was investigated, since Siemons et al. found that adding 10% alkoxy chains to an initially fully glycolated material increased its electrochemical stability.[11] This was evidenced by a slight increase in the area under the CV curve

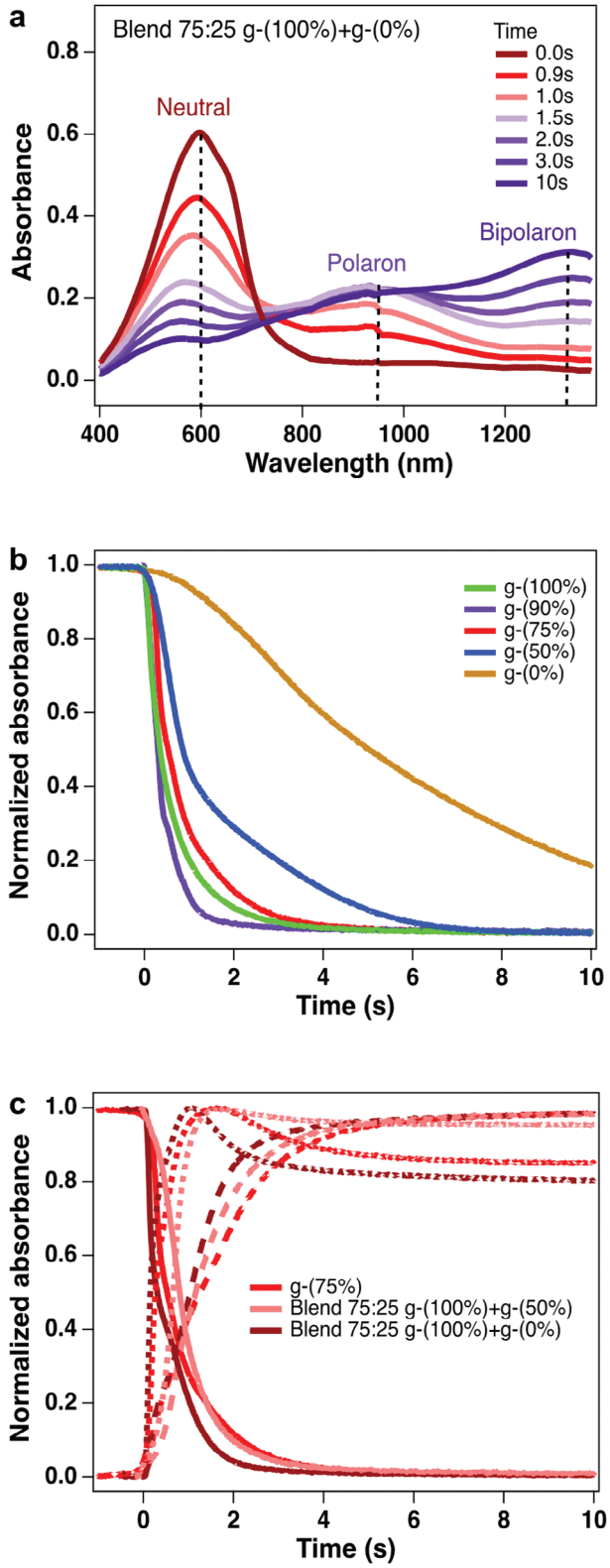

Figure 6. Oxidation dynamics in electrochemically doped copolymers and blends. a) Temporal evolution of the absorbance spectra in the type 2 blend 75:25 (g-(100%) + g-(0%)): Absorbance spectra from 0 to 10 s when switching from the dedoped state to −0.9 V in 0.1 M aqueous NaCl electrolyte. Dotted vertical lines indicate the neutral species band at ≈600 nm, the polaron species at ≈950 nm, and the bipolaron species at ≈1350 nm. b) Dynamics for the copolymers with different OEG:OR side chain ratios: Normalized absorbance (scaled between 0 and 1) at 600 nm as a function of time for g-(100%) (−0.6 V, 57 nm), g-(90%) (−0.6 V, 51 nm), g-(75%) (−0.7 V, 45 nm), g-(50%) (−0.8 V, 64 nm) and g-(0%) (−1.0 V, 58 nm) to illustrate the impact of the OEG:OR side chain ratio. Films of similar thickness were used, and in each case a voltage at −0.4 V below $V_{abs,50\%}$ (Table 1) was applied, to compare similar doping levels for the different samples. c) Oxidation dynamics in all materials with a 75:25 OEG:OR side chain ratio: Dynamics of the neutral (full lines), polaron (dotted lines), and bipolaron (dashed lines) band over time in g-(75%) and both 75:25 blends, for the same voltages as shown in (b).

for that polymer, whereas other materials in the series showed either a constant area or a slight decrease. Following the methodology of Siemons et al., electrochemical stability was assessed using a CV setup. This involved repeatedly cycling the potential against the reference electrode and analyzing changes in the area under the CV curve, which indicates the total charge accumulated in the material. In our study, all materials experienced an increase in the area under the CV curve, indicating excellent electrochemical stability (Figure S29, Supporting Information). This increase was larger for both channel materials containing 10% alkoxy side chains, in line with the results of Siemons et al.[11] Furthermore, no significant difference was found in the behavior of the copolymer and the blend with the same side chain ratio under repeated CV cycling, demonstrating that blending two polymers does not negatively impact the electrochemical stability compared to copolymerization.

Second, we investigated the OECT stability by measuring the drain current during continuous ON-OFF cycling of the OECT devices. The ON state of the OECT is specified as the gate voltage at which maximal transconductance is achieved, ≈ −0.7 V for all three systems, while the OFF state is taken at 0 V. The OECTs are cycled over 10 min at a drain voltage of −0.6 V. The OECT with g-(100%) retains over 40% of its original ON current, whereas the OECTs with the copolymer g-(90%) and the 90:10 type 1 blend, both have an ON current retention of ≈15% (Figure S30, Supporting Information). Despite the increased electrochemical stability when incorporating 10% alkoxy side chains, it seems like this is not necessarily beneficial for OECT stability. Again, it has to be noted that for the same side chain ratio, in this case 90:10 OEG:OR, very similar results are obtained, whether this ratio is achieved through copolymerization or blending techniques, further affirming the viability of blending as a more facile alternative to copolymerization.

3. Conclusion

Our findings highlight the potential of physically mixing two polymers as a strategy to rationally tailor the properties of semiconducting polymer channels in OECTs. By blending glycolated and alkoxylated polymers in specific ratios, we were able to tune the electronic and ionic properties of the channel materials effectively, achieving performance metrics comparable to those of copolymer-based systems. Our study shows that the OECT results of a copolymer series can be complicated by batch-to-batch variability, as illustrated for the g-(75%) copolymer. Conversely, blending two polymers can circumvent the synthetic complex-

Table 2. Impact of glycol side chain ratio on the oxidation dynamics: Time constants of the depletion of the neutral species absorbance band at 600 nm for copolymers and blends with varying glycol ratios. The corresponding dynamics are shown in Figures 6 and S28 (Supporting Information). Films of similar thickness were used, and in each case a voltage at −0.4 V below $V_{abs,50\%}$ was applied. Time constants were defined as the time for the normalized absorbance to reach 50% of the initial amplitude.

	$\tau_{600nm,\ Abs50\%}$ [s]				
	g-(100%)	90:10	75:25	50:50	g-(0%)
Copolymers	0.34	0.30	0.53	0.86	5.00
Type 1 blends g-(100%) + g-(50%)	–	0.16	0.81	–	–
Type 2 blends g-(100%) + g-(0%)	–	0.03	0.31	0.67	–

ity and reproducibility issues associated with copolymerization, while maintaining high μC^* values. The physical mixtures of glycolated and alkoxylated polymers exhibited controlled threshold voltages and response times and afforded the same electrochemical and OECT stability as their corresponding copolymers, demonstrating the feasibility of this approach for fine-tuning OECT properties. Generally, the blends with g-(50%) outperformed those with g-(0%), indicating that the device performance depends on the choice of polymer used to introduce the hydrophobic side chains. The type 1 blends were fully intermixed according to GIWAXS analysis and thus retained the high volumetric capacitance characteristic of fully glycolated materials but also benefited from the increased backbone planarity and reduced swelling conferred by the alkoxy side chains, as evidenced by the slightly increased electronic mobility. In summary, polymer blending emerges as a robust strategy to adapt OECT characteristics. It provides a more straightforward approach to material optimization compared to traditional copolymerization, as only two polymers are needed to create channel materials with any desired side chain ratio.

4. Experimental Section

Materials and Characterization: All reagents and chemicals were obtained from commercial sources and used without further purification. Dry solvents were obtained from a solvent purification system (MBraun, MB-SPS-800) equipped with alumina columns. Purification of the intermediates and final monomers was carried out on a Buchi Sepacore Flash Chromatography System. NMR spectra were recorded on a Jeol NMR spectrometer operating at 400 MHz for ^{1}H (100 MHz for ^{13}C). Chemical shifts (δ, in ppm) were established relative to $CDCl_3$ (δ = 7.26 ppm for ^{1}H NMR, δ = 77.16 ppm for ^{13}C NMR) or DMSO-d_6 (δ = 2.50 ppm for ^{1}H NMR). Matrix-assisted laser desorption/ionization – time-of-flight (MALDI-ToF) mass spectra were recorded on a Bruker UltrafleXtremeTM MALDI-TOF/TOF system. Sample preparation consisted of mixing 10 µL of the matrix solution (25 mg mL^{-1} *trans*-2-[3-(4-*tert*-butylphenyl)-2-methyl-2-propenylidene] malononitrile (DTCB) in chloroform) with 3 µL of the analyte solution (10 mg mL^{-1} in chloroform), after which 0.5 µL of the mixture was spotted onto an MTP Anchorchip 600/384 MALDI plate. Cyclic voltammetry was performed using an Autolab PGSTAT30 from Methrohm controlled with GPES software (version 4.9) and a standard three-electrode configuration featuring a polymer-coated ITO glass slide as the working electrode, a platinum counter electrode, and an Ag/AgCl reference electrode. The ITO glass slides were cleaned by sonication in acetone, methanol, and isopropanol, after which the polymers/blends were deposited by spin-coating 100 µL of 6 mg mL^{-1} solutions. Before performing the measurements, the layer thicknesses were determined with a Bruker Veeco Dektak XT profilometer. The CV measurements were carried out in an aqueous electrolyte, consisting of 0.1 M sodium chloride in distilled water and degassed for 10 min prior to the measurement. The scan rate at which the voltammograms were recorded was 100 mV s^{-1}. Typically, 6 scans per film were recorded and the oxidation onsets were determined for the 6th scan from the intersection of the baseline and the tangent at the point of the highest slope. Spectroelectrochemistry was performed using a home-built setup controlled by LabVIEW. Voltages are presented in the transistor convention where the source electrode (S) is grounded, such that $V_{GS} < 0$ induces doping, with the drain and gate electrodes short-circuited to prevent asymmetric doping along the channel (V_{DS} = 0). A data acquisition card (USB6211, National Instruments) was used to apply and measure the GS voltage. The GS current was converted into a voltage using a low-noise current preamplifier (SR570, Stanford Research Systems) and measured with the data acquisition card (time resolution of 8 µs). A halogen light source (HL-2000, Ocean Insight) was used to generate the incident white light. The UV-Vis-NIR absorbance spectra of polymer films in electrolyte solution were acquired with a Flame UV-Vis spectrometer and a Flame NIR spectrometer (Ocean Insight) triggered by the data acquisition card, with a time resolution of 10 ms.

OECTs: Chromium/gold (10/60 nm) drain and source contacts were thermally evaporated on ultra-flat cleaned quartz substrates. OECTs with different channel dimensions were tested by using substrates containing 2 transistors, T1 (L x W = 2 × 3 mm) and T2 (L x W = 0.5 × 5.5 mm), as well as preparing channels with different thickness. The polymers/blends were deposited by spin-coating 100 µL of the respective solutions in $CHCl_3$ at 1500 rpm for 1 min. Solutions of different concentrations were used to obtain a variety of film thicknesses, which were measured using a Bruker Contour GT-K optical profiler using light interferometry (green light, PSI mode) controlled by Vision 64 software. Calibration curves were made to show that the absorbance is linearly dependent on thickness. Each value used for the calibration curve is the average of 4–6 thickness measurements. The channel dimensions were defined by wiping away all excess material with a cotton swab, after which the substrate was placed in a closed cell. Prior to the experiment, the electrolyte, a 0.1 M sodium chloride solution in distilled water, was degassed by nitrogen bubbling for 10 min and then injected in the cell. Transfer and output characteristics were obtained using a home-built setup controlled by LabVIEW. Voltages are given in transistor convention where the source electrode is grounded, i.e. $V_{GS} < 0$ induces p-doping. All transfer characteristics were performed on pre-cycled (3x) OECTs. V_{DS} was applied using a Keithley 2400 SMU (Tektronix) and fixed at −0.6 V prior to applying V_{GS}. Then, V_{GS} was applied using a data acquisition system (USB-6211 from National Instrument Corp.) and swept back and forth from 0.1 to −0.6 V and back to 0.1 V at a scan rate of 10 mV s^{-1}. The resulting I_{DS} was recorded with the same Keithley 2400 SMU. All output characteristics were performed after acquiring the transfer curves. A fixed V_{GS} was applied using a data acquisition system (USB-6211 from National Instrument Corp.) and decreased stepwise from −0.1 to −0.6 V (ΔV = −0.1 V). V_{DS} was swept using a Keithley 2400 SMU (Tektronix) from 0 to −0.6 V at a scan rate of 10 mV s^{-1}. The resulting I_{DS} was recorded with the Keithley 2400 SMU.

Chronoamperometry: Chronoamperometry measurements were conducted on films deposited on ITO substrates using a degassed 0.1 M aqueous NaCl electrolyte in contact with a Ag/AgCl electrode. The gate-source current (I_{GS}) was recorded in response to square voltage pulses (V_{GS}) applied to the system. These voltage pulses varied from +0.6 to −0.8 V in steps of 0.1 V, with each step maintained for a duration of 30 s to record the current transients. The data analysis involved integrating the current over time to estimate the total injected charge. The volumetric capacitance (C^*) was then determined by analyzing the slope of the carrier density as a function of the applied voltage, particularly focusing on those above the

threshold voltage. The transient response gate-source current (I_{GS}) was converted to voltage using a low noise current preamplifier (SR570, Stanford Research Systems) and this voltage was measured with the USB 6008 data acquisition card.

GIWAXS: Samples were spin-coated at 1000 rpm onto a native oxide silicon substrate from a 10 mg mL^{-1} solution in $CHCl_3$. GIWAXS measurements were performed at the Stanford Synchrotron Radiation Lightsource on beamline 11–3, with an X-ray energy of 12.7 keV and an incidence angle of 0.1°. The sample-to-detector distance was 309.1 mm and calibrated to a polycrystalline LaB6 standard. Measurements were performed in a helium chamber to minimize air scattering. All data were corrected for the geometric distortion of the flat detector used, normalized by exposure time, sample thickness, and monitor counts, and analyzed using Nika 1D SAXS1[39] and WAXstools[40] software in Igor Pro.[39] Lineouts were taken at azimuthal angle ranges of −25 to +25° and 70 to 88° for the Q_z and Q_{xy} lineouts.

Electrochemical and OECT Stability Measurements: The electrochemical stability was determined using the CV experiment as explained in the materials and characterization section. The potential vs. the Ag/AgCl reference electrode was swept between −0.5 and +0.5 V for 500 consecutive cycles and the changes in the area under the curves of the resulting voltammograms were used to draw conclusions regarding stability.

The OECTs for the stability measurements were fabricated similarly to the OECTs used for the other performance measurements (OECTs section). Chromium/gold (20/80 nm) drain and source contacts were thermally evaporated on cleaned borosilicate glass, creating OECT channels with dimensions LxW = 0.5 × 6 mm. The polymers/blends were deposited by spin-coating 100 µL of the respective solutions in $CHCl_3$ (5 mg mL^{-1}) at 1000 rpm for 1 min and the channel dimensions were defined by wiping away all excess material with a cotton swab. The Ag/AgCl gate electrode (A-M systems) was submerged in a 0.1 M NaCl electrolyte solution, contained within a PDMS well on top of the OECT channel, in ambient conditions. The OECT stability was determined by measuring the drain current during the continuous ON-OFF cycling of the OECT devices, alternating the gate voltage between 0 and −0.7 V over 10 min (each cycle comprising ≈22 s) while the OECT channel was biased at a constant drain voltage of −0.6 V. Two Keithley 2400 SMU (Tektronix) were used to apply the drain/gate voltage and record the resulting drain/gate current, controlled by custom LabVIEW software.

Vis/NIR Spectroelectrochemistry in OECTs and Thin Films on ITO Substrates: The spectroelectrochemical optical measurements were carried out using a custom-designed setup to capture the absorbance spectra with a time resolution of 5–10 ms. Films on ITO substrates submerged in a degassed 0.1 M aqueous NaCl electrolyte solution were measured, as well as OECTs, to compare the two configurations. The in situ Vis-NIR absorbance setup includes a halogen light source (HL-2000, Ocean Insight) and Flame UV–vis and Flame NIR spectrometers (Ocean Insight). The light is focused on the sample and transmits through a 2 mm path length of electrolyte and the active transistor channel before it is focused and collected by the spectrometers. The system is controlled and synchronized using a digital delay/pulse generator (DG535, Stanford Research Systems) and a custom LabVIEW code ensuring accurate timing and data collection. The voltage application between the Ag/AgCl electrode and the polymer-coated ITO substrates was conducted using a data acquisition card (USB-6008, National Instruments, time resolution of 5–10 ms). In this setup, the Ag/AgCl quasi-reference electrode is connected to the voltage source, while the polymer-coated ITO substrates were grounded. Before the actual measurements, the polymer/blend films underwent a pre-cycling process four times. Each pre-cycling step involves applying a −0.8 V voltage pulse for 100 s to dope the polymer, followed by a +0.5 V or +0.6 V pulse for 100 s to dedope it. Time-resolved measurements were then conducted by applying 100 s square voltage pulses to alternatively dope and dedope the polymer. The doping voltage ranged from +0.6 to −0.8 V in −0.1 V steps, and the dedoping bias was consistently set at +0.6 V.

EQCM-D: EQCM-D measurements were performed using a Q-Sense analyzer (QE401, Biolin Scientific) with Cr/Au-coated quartz crystals sensors (area of 0.7854 cm^2) and a Qsense module (QEM 401) with an Ag/AgCl reference and platinum counter electrode. First, the bare sensors, that were used as a reference, were measured in air and in NaCl 0.1 M aqueous electrolyte (flow rate of 50 µL min^{-1}). Then, the sensors were coated with the copolymer and blend solutions (3 mg mL^{-1} in $CHCl_3$). Next, the measurement protocol was repeated for the coated sensors. For each step, we waited long enough until the frequency and dissipation were stabilized ($\Delta f < 0.1$Hz per 5 min). The films were biased using a VMP-003 Biologic potentiostat. For each material, we first recorded the OCV and then performed three CV cycles at a scan rate of 50 mV s^{-1} followed by chronoamperometry steps ranging from -0.1 to -0.6 V vs OCV. After each step, the film was dedoped at 0 V vs OCV. The Saurbrey equation was used to convert the shifts into mass. The swelling is defined as the percentage change in volume relative to the dry film, as follows: Swelling = $(V_{tot} - V_{dry})/V_{dry} * 100\%$.

Supporting Information

Supporting Information is available from the Wiley Online Library or from the author.

Acknowledgements

This project received funding from the European Union's Horizon 2020 Research and Innovation Program under grant agreement no. 964677 (MITICS). W.M., K.V., L.B., J.V., and A.G. thank the FWO Vlaanderen for financial support (WEAVE project G025922N and Ph.D. grants 1S70122N and 1S50820N). K.Z., N.B., and D.T. acknowledge the Swiss National Science Foundation (grant 200021E_205216) and the University of Bern for funding. We also thank O. Bardagot for helpful discussions on OECT measurements and data analysis. Use of the Stanford Synchrotron Radiation Light source, SLAC National Accelerator Laboratory, is supported by the U.S. Department of Energy, Office of Science, Office of Basic Energy Sciences, under Contract No. DE-AC02-76SF00515.

Open access publishing facilitated by Universitat Bern, as part of the Wiley - Universitat Bern agreement via the Consortium Of Swiss Academic Libraries.

Conflict of Interest

The authors declare no conflict of interest.

Author Contributions

L.B. synthesized and characterized the materials, and performed MALDI-ToF MS, UV–vis, CV, and OECT measurements and data analysis. K.Z. performed the chronoamperometry measurements and determined *C**, obtained the steady-state and time-resolved spectroelectrochemistry data, and did the kinetic analysis. P.C. and T.C.H.C. performed EQCM-D measurements and T.C.H.C. conducted data analysis, under the supervision of S.I. P.C. also assisted in the OECT measurements and data analysis. A.G. performed the OECT stability measurements and data analysis. D.T. assisted in the kinetic analysis. J.V. was involved in the conceptualization, materials synthesis, and polymer characterization and analyzed the GIWAXS data. Ad.M. and K.W. performed the ICP-MS measurements and data analysis. Ad. M and Ar.M performed the GIWAXS measurements and assisted in data interpretation. L.L. was involved in overall project and student supervision. K.V. supervised the stability measurements and contributed to the discussions. N.B. supervised the OECT device measurements, the spectroelectrochemical work, and the kinetic analysis, as well as part of the overall project. W.M. supervised the materials synthesis and characterization work, and was in charge of the overall project. L.B. wrote and coordinated the manuscript, while the spectroelectrochemical and EQCM-D part was written by K.Z. and N.B. All authors contributed to the revision and editing of the manuscript.

Data Availability Statement

The data that support the findings of this study are available from the corresponding authors upon reasonable request. The data that support the findings of this work and were gathered at the University of Bern are available as open access in the BORIS Repository of the University of Bern at https://boris-portal.unibe.ch/handle/20.500.12422/204283.

Keywords

copolymerization, glycol and alkoxy side chains, organic electrochemical transistors, polymer blends, semiconducting polymers

Received: January 2, 2025
Revised: January 20, 2025
Published online: February 7, 2025

[1] S. G. Higgins, A. Lo Fiego, I. Patrick, A. Creamer, M. M. Stevens, *Adv. Mater. Technol.* **2020**, *5*, 2000384.
[2] J. Rivnay, S. Inal, A. Salleo, R. M. Owens, M. Berggren, G. G. Malliaras, *Nat. Rev. Mater.* **2018**, *3*, 17086.
[3] a) Q. Thiburce, N. Melosh, A. Salleo, *Flex. Print. Electron.* **2022**, *7*, 034001; b) A. Makhinia, L. Bynens, A. Goossens, J. Deckers, L. Lutsen, K. Vandewal, W. Maes, V. Beni, P. Andersson Ersman, *Adv. Funct. Mater.* **2024**, 2314857; c) A. Nag, S. C. Mukhopadhyay, J. Kosel, *IEEE Sens. J.* **2017**, *17*, 3949.
[4] J. T. Friedlein, R. R. McLeod, J. Rivnay, *Org. Electron.* **2018**, *63*, 398.
[5] A. Giovannitti, R. B. Rashid, Q. Thiburce, B. D. Paulsen, C. Cendra, K. Thorley, D. Moia, J. T. Mefford, D. Hanifi, D. Weiyuan, M. Moser, A. Salleo, J. Nelson, I. McCulloch, J. Rivnay, *Adv. Mater.* **2020**, *32*, 1908047.
[6] M. Moser, J. F. Ponder, A. Wadsworth, A. Giovannitti, I. McCulloch, *Adv. Funct. Mater.* **2018**, *29*, 1807033.
[7] a) A. Giovannitti, D. T. Sbircea, S. Inal, C. B. Nielsen, E. Bandiello, D. A. Hanifi, M. Sessolo, G. G. Malliaras, I. McCulloch, J. Rivnay, *Proc. Natl. Acad. Sci. U S A* **2016**, *113*, 12017; b) N. Siemons, D. Pearce, C. Cendra, H. Yu, S. M. Tuladhar, R. K. Hallani, R. Sheelamanthula, G. S. LeCroy, L. Siemons, A. J. P. White, I. McCulloch, A. Salleo, J. M. Frost, A. Giovannitti, J. Nelson, *Adv. Mater.* **2022**, *34*, 2204258; c) Y. He, N. A. Kukhta, A. Marks, C. K. Luscombe, *J. Mater. Chem. C* **2022**, *10*, 2314.
[8] a) H. Jia, Z. Huang, P. Li, S. Zhang, Y. Wang, J.-Y. Wang, X. Gu, T. Lei, *J. Mater. Chem. C* **2021**, *9*, 4927; b) M. Moser, A. Savva, K. Thorley, B. D. Paulsen, T. C. Hidalgo, D. Ohayon, H. Chen, A. Giovannitti, A. Marks, N. Gasparini, A. Wadsworth, J. Rivnay, S. Inal, I. McCulloch, *Angew. Chem. Int. Ed. Engl.* **2021**, *60*, 7777.
[9] S. Moro, N. Siemons, O. Drury, D. A. Warr, T. A. Moriarty, L. M. A. Perdigao, D. Pearce, M. Moser, R. K. Hallani, J. Parker, I. McCulloch, J. M. Frost, J. Nelson, G. Costantini, *ACS Nano* **2022**, *16*, 21303.
[10] B. Ding, I. Y. Jo, H. Yu, J. H. Kim, A. V. Marsh, E. Gutierrez-Fernandez, N. Ramos, C. L. Rapley, M. Rimmele, Q. He, J. Martin, N. Gasparini, J. Nelson, M. H. Yoon, M. Heeney, *Chem. Mater.* **2023**, *35*, 3290.
[11] N. Siemons, D. Pearce, H. Yu, S. M. Tuladhar, G. S. LeCroy, R. Sheelamanthula, R. K. Hallani, A. Salleo, I. McCulloch, A. Giovannitti, J. M. Frost, *J. Nelson, Proc. Natl. Acad. Sci. U S A* **2023**, *120*, 2306272120.
[12] a) J. Guo, S. E. Chen, R. Giridharagopal, C. G. Bischak, J. W. Onorato, K. Yan, Z. Shen, C.-Z. Li, C. K. Luscombe, D. S. Ginger, *Nat. Mater.* **2024**, *23*, 656; b) S. T. Keene, J. E. M. Laulainen, R. Pandya, M. Moser, C. Schnedermann, P. A. Midgley, I. McCulloch, A. Rao, G. G. Malliaras, *Nat. Mater.* **2023**, *22*, 1121; c) P. R. Paudel, M. Skowrons, D. Dahal, R. K. Radha Krishnan, B. Lüssem, *Adv. Theory Simul.* **2022**, *5*, 2100563; d) M. Skowrons, A. Schander, A. G. P. Negron, B. Lüssem, *Adv. Electron. Mater.* **2024**, *10*, 2300673.
[13] A. Savva, R. Hallani, C. Cendra, J. Surgailis, T. C. Hidalgo, S. Wustoni, R. Sheelamanthula, X. Chen, M. Kirkus, A. Giovannitti, A. Salleo, I. McCulloch, S. Inal, *Adv. Funct. Mater.* **2020**, *30*, 1907657.
[14] a) S. E. Chen, L. Q. Flagg, J. W. Onorato, L. J. Richter, J. Guo, C. K. Luscombe, D. S. Ginger, *J. Mater. Chem. A* **2022**, *10*, 10738; b) B. T. DiTullio, L. R. Savagian, O. Bardagot, M. De Keersmaecker, A. M. Osterholm, N. Banerji, J. R. Reynolds, *J. Am. Chem. Soc.* **2023**, *145*, 122; c) M. Moser, J. Gladisch, S. Ghosh, T. C. Hidalgo, J. F. Ponder, R. Sheelamanthula, Q. Thiburce, N. Gasparini, A. Wadsworth, A. Salleo, S. Inal, M. Berggren, I. Zozoulenko, E. Stavrinidou, I. McCulloch, *Adv. Funct. Mater.* **2021**, *31*, 2100723; d) M. Moser, L. R. Savagian, A. Savva, M. Matta, J. F. Ponder, T. C. Hidalgo, D. Ohayon, R. Hallani, M. Reisjalali, A. Troisi, A. Wadsworth, J. R. Reynolds, S. Inal, I. McCulloch, *Chem. Mater.* **2020**, *32*, 6618; e) M. Moser, Y. Wang, T. C. Hidalgo, H. Liao, Y. Yu, J. Chen, J. Duan, F. Moruzzi, S. Griggs, A. Marks, N. Gasparini, A. Wadsworth, S. Inal, I. McCulloch, W. Yue, *Mater. Horiz.* **2021**, 973; f) J. W. Onorato, Z. Wang, Y. Sun, C. Nowak, L. Q. Flagg, R. Li, B. X. Dong, L. J. Richter, F. A. Escobedo, P. F. Nealey, S. N. Patel, C. K. Luscombe, *J. Mater. Chem. A* **2021**, *9*, 21410; g) P. Schmode, A. Savva, R. Kahl, D. Ohayon, F. Meichsner, O. Dolynchuk, T. Thurn-Albrecht, S. Inal, M. Thelakkat, *ACS Appl. Mater. Interfaces* **2020**, *12*, 13029; h) J. Tropp, D. Meli, R. Wu, B. Xu, S. B. Hunt, J. D. Azoulay, B. D. Paulsen, J. Rivnay, *ACS Mater. Lett.* **2023**, *5*, 1367.
[15] J. Kimpel, Y. Kim, J. Asatryan, J. Martin, R. Kroon, C. Muller, *Chem. Sci.* **2024**, *15*, 7679.
[16] a) J. Vanderspikken, Z. Liu, X. C. Wu, O. Beckers, S. Moro, T. J. Quill, Q. Liu, A. Goossens, A. Marks, K. Weaver, M. Hamid, B. Goderis, E. Nies, V. Lemaur, D. Beljonne, A. Salleo, L. Lutsen, K. Vandewal, B. Van Mele, G. Costantini, N. Van den Brande, W. Maes, *Adv. Funct. Mater.* **2023**, *33*, 2309403; b) Z. Liu, J. Vanderspikken, P. Mantegazza, S. Moro, M. Hamid, S. Mertens, N. Van den Brande, L. Lutsen, V. Lemaur, D. Beljonne, G. Costantini, K. Vandewal, B. Van Mele, W. Maes, B. Goderis, *Adv. Funct. Mater.* **2024**, 2413647.
[17] S. Griggs, A. Marks, D. Meli, G. Rebetez, O. Bardagot, B. D. Paulsen, H. Chen, K. Weaver, M. I. Nugraha, E. A. Schafer, J. Tropp, C. M. Aitchison, T. D. Anthopoulos, N. Banerji, J. Rivnay, I. McCulloch, *Nat. Commun.* **2022**, *13*, 7964.
[18] M. Barker, T. Nicolini, Y. A. Yaman, D. Thuau, O. Siscan, S. Ramachandran, E. Cloutet, C. Brochon, L. J. Richter, O. J. Dautel, G. Hadziioannou, N. Stingelin, *Mater. Horiz.* **2023**, *10*, 248.
[19] E. Stein, O. Nahor, M. Stolov, V. Freger, I. M. Petruta, I. McCulloch, G. L. Frey, *Nat. Commun.* **2022**, *13*, 5548.
[20] I. McCulloch, M. Heeney, C. Bailey, K. Genevicius, I. Macdonald, M. Shkunov, D. Sparrowe, S. Tierney, R. Wagner, W. Zhang, M. L. Chabinyc, R. J. Kline, M. D. McGehee, M. F. Toney, *Nat. Mater.* **2006**, *5*, 328.
[21] R. K. Hallani, B. D. Paulsen, A. J. Petty, R. Sheelamanthula, M. Moser, K. J. Thorley, W. Sohn, R. B. Rashid, A. Savva, S. Moro, J. P. Parker, O. Drury, M. Alsufyani, M. Neophytou, J. Kosco, S. Inal, G. Costantini, J. Rivnay, I. McCulloch, *J. Am. Chem. Soc.* **2021**, *143*, 11007.
[22] J. Vanderspikken, Q. Liu, Z. Liu, T. Vandermeeren, T. Cardeynaels, S. Gielen, B. Van Mele, N. Van den Brande, B. Champagne, K. Vandewal, W. Maes, *Adv. Funct. Mater.* **2021**, *32*, 2108146.
[23] a) K. Gu, J. Onorato, S. S. Xiao, C. K. Luscombe, Y.-L. Loo, *Chem. Mater.* **2018**, *30*, 570; b) A. Giovannitti, I. P. Maria, D. Hanifi, M. J. Donahue, D. Bryant, K. J. Barth, B. E. Makdah, A. Savva, D. Moia, M. Zetek, P. R. F. Barnes, O. G. Reid, S. Inal, G. Rumbles, G. G. Malliaras, J. Nelson, J. Rivnay, I. McCulloch, *Chem. Mater.* **2018**, *30*, 2945.
[24] J. Vanderspikken, P. Verstappen, W. Maes, *Macromolecules* **2024**, *57*, 7138.
[25] a) K. J. Wu, R. W. Odom, *Anal. Chem.* **1998**, *70*, 456A; b) T. J. Quill, G. LeCroy, A. Marks, S. A. Hesse, Q. Thiburce, I. McCulloch, C. J.

Tassone, C. J. Takacs, A. Giovannitti, A. Salleo, *Adv. Mater.* **2024**, 2310157.
[26] H. C. Michelle Byrd, C. N. McEwen, *Anal. Chem.* **2000**, *72*, 4568.
[27] a) V. Vijayakumar, Y. Zhong, V. Untilova, M. Bahri, L. Herrmann, L. Biniek, N. Leclerc, M. Brinkmann, *Adv. Energy Mater.* **2019**, *9*, 1900266; b) K. Zhou, Y. Liu, Y. Xu, H. Wu, X. Zhou, K. Chen, X. Xu, Z. Ma, Z. Tang, W. Ma, *J. Mater. Chem. C* **2021**, *9*, 13761.
[28] K. Kang, S. Watanabe, K. Broch, A. Sepe, A. Brown, I. Nasrallah, M. Nikolka, Z. Fei, M. Heeney, D. Matsumoto, K. Marumoto, H. Tanaka, S. Kuroda, H. Sirringhaus, *Nat. Mater.* **2016**, *15*, 896.
[29] D. A. Bernards, G. G. Malliaras, *Adv. Funct. Mater.* **2007**, *17*, 3538.
[30] S. Inal, G. G. Malliaras, J. Rivnay, *Nat. Commun.* **2017**, *8*, 1767.
[31] M. Shahi, V. N. Le, P. Alarcon Espejo, M. Alsufyani, C. J. Kousseff, I. McCulloch, A. F. Paterson, *Nat. Mater.* **2024**, *23*, 2.
[32] H. J. Kim, K. Perera, Z. Liang, B. Bowen, J. Mei, B. W. Boudouris, *ACS Macro Lett* **2022**, *11*, 243.
[33] A. F. Paterson, A. Savva, S. Wustoni, L. Tsetseris, B. D. Paulsen, H. Faber, A. H. Emwas, X. Chen, G. Nikiforidis, T. C. Hidalgo, M. Moser, I. P. Maria, J. Rivnay, I. McCulloch, T. D. Anthopoulos, S. Inal, *Nat. Commun.* **2020**, *11*, 3004.
[34] J. Surgailis, A. Savva, V. Druet, B. D. Paulsen, R. Wu, A. Hamidi-Sakr, D. Ohayon, G. Nikiforidis, X. Chen, I. McCulloch, J. Rivnay, S. Inal, *Adv. Funct. Mater.* **2021**, *31*, 2010165.
[35] O. Bardagot, N. Banerji, *Chimia (Aarau)* **2022**, *76*, 546.
[36] A. I. Hofmann, R. Kroon, S. Zokaei, E. Järsvall, C. Malacrida, S. Ludwigs, T. Biskup, C. Müller, *Adv. Electron. Mater.* **2020**, *6*, 2000249.
[37] a) D. Tsokkou, P. Cavassin, G. Rebetez, N. Banerji, *Mater. Horiz.* **2022**, *9*, 482; b) S. Züfle, S. Altazin, A. Hofmann, L. Jäger, M. T. Neukom, W. Brütting, B. Ruhstaller, *J. Appl. Phys.* **2017**, *122*, 115502.
[38] A. Giri, Y. Khakre, G. Shreeraj, T. K. Dutta, S. Kundu, A. Patra, *J. Mater. Chem. A* **2022**, *10*, 17077.
[39] J. Ilavsky, *J. Appl. Crystallogr.* **2012**, *45*, 324.
[40] S. D. Oosterhout, V. Savikhin, J. Zhang, Y. Zhang, M. A. Burgers, S. R. Marder, G. C. Bazan, M. F. Toney, *Chem. Mater.* **2017**, *29*, 3062.